

Exploiting Variable Impedance for Energy Efficient Sequential Movements

Journal Title
XX(X):1–15
©The Author(s) 2020
Reprints and permission:
sagepub.co.uk/journalsPermissions.nav
DOI: 10.1177/ToBeAssigned
www.sagepub.com/

SAGE

Fan Wu^{1 2} and Matthew Howard²

Abstract

Compliant robotics have seen successful applications in energy efficient locomotion and cyclic manipulation. However, exploitation of variable physical impedance for energy efficient sequential movements has not been extensively addressed. This work employs a hierarchical approach to encapsulate low-level optimal control for sub-movement generation into an outer loop of iterative policy improvement, thereby leveraging the benefits of both optimal control and reinforcement learning. The framework enables optimizing efficiency trade-off for minimal energy expenses in a model-free manner, by taking account of cost function weighting, variable impedance exploitation, and transition timing — which are associated with the skill of compliance. The effectiveness of the proposed method is evaluated using two consecutive reaching tasks on a variable impedance actuator. The results demonstrate significant energy saving by improving the skill of compliance, with an electrical consumption reduction of about 30% measured in a physical robot experiment.

Keywords

sequential movements, energy efficiency, variable impedance actuators, optimal control, reinforcement learning, evolution strategies

1 Introduction

Intrinsically compliant robots typically have elastic components for stiffness modulation and such elements are capable of storing elastic energy. The field of robotic locomotion has seen a series of successful developments of energy efficient robots with elastic joints or springy legs that can exploit this energy storage. It is of great interest to apply the same principle to robotic manipulators such that soft robots can behave in a human-like energy efficient way for a wide variety of tasks.

Biological springs, like tendons and various elastic elements in muscles, are embedded in humans and animals and make them highly efficient runners and jumpers (Roberts (2016)). Utilizing elastic energy storage and recoil, which is associated with optimizing muscular stiffness and transition timing, is a crucial skill that can be practised and improved for many other athletic activities, not limited to locomotion (Wilson and Flanagan (2008)).

Physical compliance incorporating elastic components is prominent for energy efficient lower limb locomotion (Reher et al. (2016); Roozing et al. (2016, 2019)). Also, they have been demonstrated to reproduce the skill of *energy buffering* in explosive movements such as throwing (Wolf and Hirzinger (2008); Braun et al. (2013)). Storing and discharging elastic energy, which was called as “skill of compliance” by Okada et al. (2002), can amplify the output power, exceeding the power limit of the drive motor. Other recent studies attempt to improve energy efficiency for cyclic manipulation tasks, *e.g.*, repetitive pick-and-place (Matsusaka et al. (2016)) and dribbling a basketball (Haddadin et al. (2018)).

However, many tasks in unstructured environments are not periodic and *variable physical impedance* is hard to fully exploit. For instance, the objects to be picked and placed may be located at random positions. The task given to a robot may consist of a sequence of different types of actions, such as “reach a cup, grasp it, and pour the water”. These non-periodic but *sequential* tasks more commonly involve upper limbs and are complicated by their greater diversity. The problem of task-oriented sequential movement generation — in the context of compliant robotics — faces the difficulty imposed by inherent actuation redundancy. The control redundancy of the actuators, which is somehow equivalent to the muscle redundancy of musculoskeletal arms, makes it non-trivial to optimize the movements in the “muscle space”.

Energetic economy is of great importance to reproduce human-like skilled movements. Researchers have embraced the notions of movement economy or efficiency since 1980s to understand and model human neuromuscular control of skilled movements (Nelson (1983); Sparrow and Newell (1998); Todorov and Jordan (2002)). The emergence and learning of complex motor skills can be explained as an optimization process aiming at minimizing metabolic energy expenditure subject to task, environment and organism constraints. Reduction of metabolic cost of

¹Technical University of Munich, Germany

²King's College London, UK

Corresponding author:

Fan Wu, Munich School of Robotics and Machine Intelligence, Technical University of Munich, Munich, 80797, Germany.

Email: f.wu@tum.de

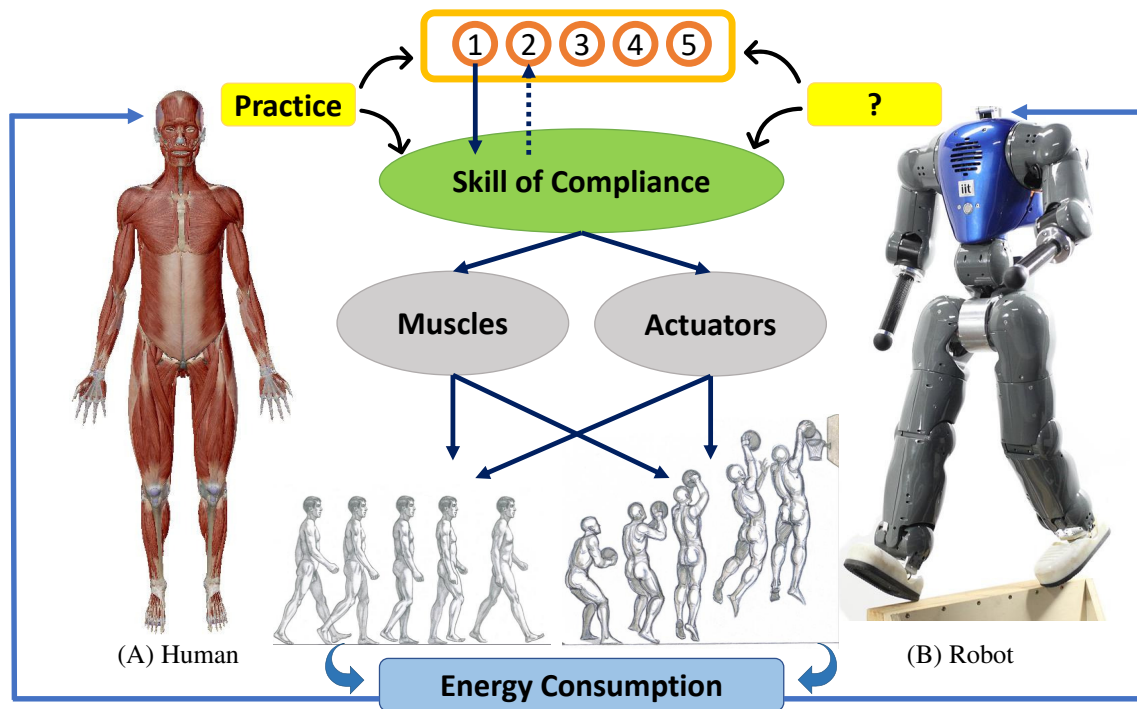


Figure 1. Conceptual diagram of energy efficient sequential movements.¹ (A) A human, and (B) a compliant humanoid robot COMAN developed by Tsagarakis et al. (2013). A task is represented by a sequence of submovements illustrated by orange circles. When one of the submovements is triggered (circle "1" in the figure), humans can use the skill of compliance — modulation of elastic energy storage and muscular stiffness — to improve the performance and energy efficiency of subsequent actions (denoted by the dashed arrow pointing to circle "2"). The same strategy can be realized by robots with physical compliance. Humans can minimize the energy consumption of skilled movements via practice, resulting in improved movement representations and associated muscle skills. However, how physical compliance can be fully exploited to minimize energy cost for sequential movements still remains an under-explored question.

human movements during training and practice has been verified by empirical studies (Lay et al. (2002); Huang et al. (2012)). However, for robots driven by variable impedance actuators (VIAs) which are viewed as the mechanical counterparts of humans and animals, there lacks a systematic optimal control approach to optimize energy efficiency of complex skills modelled as sequential movements (the analogy between humans and compliant robots in terms of energy efficient sequential movements is depicted in Figure 1). To address this, our work postulates that such a framework should consider the following aspects:

1. **Cost function weighting.** Optimization of the weighting parameters of individual cost functions to achieve a higher level objective, *e.g.*, minimal energy consumption.²
2. **Variable impedance exploitation.** A movement can adjust physical impedance (alongside the trajectory and at the transition phase) to improve its subsequent movements.
3. **Relative timing.** Temporal characteristics affect the energy efficiency. For instance, given a time horizon for the whole movement sequence, the relative timing of submovements is of importance for skilled efficient movements.

These three issues have been addressed in part in the literature. For example, inverse optimal control or inverse reinforcement learning is capable of learning the cost function from human demonstration (Mombaur et al.

(2010); Berret et al. (2011); Levine and Koltun (2012)). Nakanishi et al. (2016) exploited variable stiffness actuation for *multiphase* movements by optimal control, where a brachiation task is used for demonstration. Nakanishi et al. (2011) extended optimal control (OC) to include optimization of movement durations. An analogue via approximate inference was provided in Rawlik et al. (2010). Other works focus on optimizing the sub-goals or attractors of movements encoded by dynamical systems (Toussaint et al. (2007); Stulp et al. (2012)).

However, rarely have existing approaches addressed the above targets in the sequential context within one framework. Also, many optimization-based methods rely on combining cost functions of subtasks into a composite one, which intensifies the cost function shaping issue — requirement of redesigning the forms of cost functions — when competing terms join together.

Therefore, this paper proposes a hierarchical approach that is capable of optimizing the three aspects identified above and mitigate the cost function shaping issue. More specifically, a bi-level structure is employed to encapsulate a low-level OC layer for submovement generation into an outer loop of iterative policy improvement, thereby benefits of both OC and RL are leveraged. The high-level optimization formulated as a reinforcement learning problem enables optimizing the trade-off balance concerning (low-level) (1) cost function weighting, (2) variable impedance exploitation and (3) transition timing for minimal *realistic* energetics. The

associated high-level policy parameters can be optimized in a derivative-free fashion by a black-box optimization (BBO) method for policy improvement suggested by Stulp and Sigaud (2013). It can be viewed as a simplification of the RL algorithm PI^2 (Theodorou et al. (2010)), which closely resembles an evolution strategy (ES) (μ, λ) -ES, the backbone of CMA-ES algorithm (Hansen and Ostermeier (2001)). At the low-level OC naturally resolves the actuation redundancy and exploit variable impedance of VIAs (Braun et al. (2012, 2013)), for which there exists efficient solvers *e.g.*, Iterative Linear Quadratic Regulator (Li and Todorov (2004); Tassa et al. (2014)).

The rest of this paper is organized as follows. In §2 we discuss relevant literature and concepts. §3 first introduces a simple OC example of point-to-point reaching on the single joint VIA. By investigating the *efficient frontiers* of the OC problem we show how the hyper-parameters is identified and how the reinforcement learning problem is formulated. The proposed method is introduced in §4. Its effectiveness is evaluated by consecutive reaching tasks on a real VIA robot. Simulations demonstrate significant energy efficiency improvement and a reduction of electrical consumption of about 30% is recorded on the hardware. Conclusions and future works are covered in §6.

2 Related Work

2.1 Sequential Movements

Sequential movements are common found in human daily life, from jaw movement for speech, finger movement for playing musical instruments, to many athletic whole body actions. How can these skilful human movements be learnt, executed and improved? Central to that is whether a hierarchical structure of representation, learning and control of movement sequences exists in the human brain. The hypothesis of hierarchical organization of movement planning was proposed a long time ago in mid twentieth century by behaviourist Karl Lashley (Lashley (1951)). Recent experimental studies have provided evidence of hierarchical representation of movement sequences in the brain. For instance, Yokoi and Diedrichsen (2019) found that individual finger presses are represented in the primary motor cortex, whereas activities about the sequential context happen mainly in the premotor and parietal cortices.

In the robotics literature, sequential composition of controllers was employed by Burrige et al. (1999) to achieve dynamically dexterous robot behaviours. In robot learning control, motion generation of complex skills is often investigated at the task level and treated in a hierarchical manner. A complex skill can be learnt from human demonstrations by motion segmentation into movement primitives (Lucia et al. (2013)). Then a skilful movement can be composed by a “repertoire” (Schaal and Atkeson (2010)) of such sequenced submovements. By doing so it is expected to realize more general motion intelligence and make robots master interactive tasks and tool use, which is a hallmark of human behaviour (Hogan and Sternad (2012)).

Humans can acquire a new skilled movement by sequencing simpler motion primitives and improving via practice. Although each individual movement can be fine-tuned during training, the increased performance through

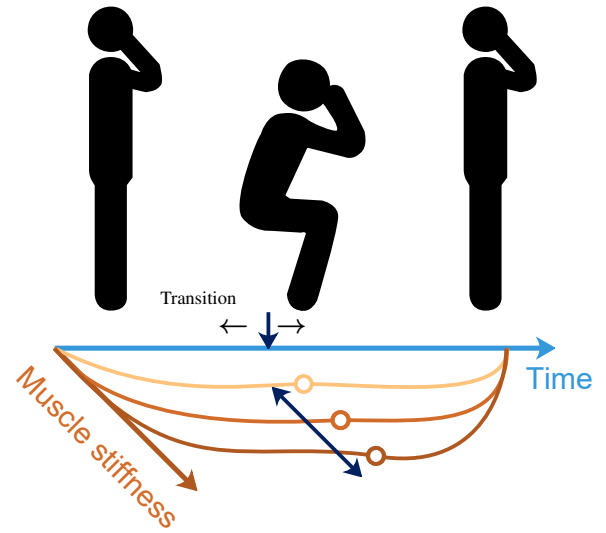


Figure 2. Humans can acquire new skilled movement by sequencing simpler motion primitives. A squat can be composed of crouching and rising-up, and the corresponding variables in the sequential context can be improved through practice. Possible ways to optimize the squat towards higher energy efficiency are: (i) adjust transition timing, and (ii) modulate muscular stiffness.

practice can be clearly attributed to improvements in high-level planning processes, as shown by Ariani and Diedrichsen (2019). For example, consider a squat (see Figure 2) that can be composed of crouching and rising-up. By intuition, the contextual variables at the sequence planning level can possibly be transition timing, muscular stiffness, torque distribution, *etc.* Moteji and Matsui (2011) used OC to find optimal transition timing that can reproduce experimentally measured human squat movements. The role of stiffness was investigated by Bobbert (2001) also through biomechanical modelling and OC, which signifies the importance of *exploiting elastic energy storage*.

2.2 Optimization of Sequential Movements

Improvement of a sequential movement necessitates existence of redundancy in either representational level or control level. In the above squat example, the transition timing is not predefined by the task or sub-movements, and thus can be tuned. While for playing a piece of music, the tempo and rhythm are determined, then the transition timing is specified by the task objective and cannot be exploited.

It is easy to notice that sequentially combining the sub-movements, which are optimized with respect to their sub-goals, does not necessarily result in the optimal movement for the whole task. Look at the example illustrated in Figure 3, the minimal-jerk trajectory (Flash and Hogan (1985)) of a via-point task from point A to C via B (at a specific time) results in a curved path in the X-Y plane. While the minimal-jerk model of a single point-to-point movement always shows a straight path. Consequently, if we sequence AB and BC (both individually are minimal-jerk) directly, the resulting trajectory is not optimal in terms of the whole movement. The difference is simply due to that the velocity at the via point is not constrained to be zero. Though it is obvious, this common phenomenon in kinematic domain

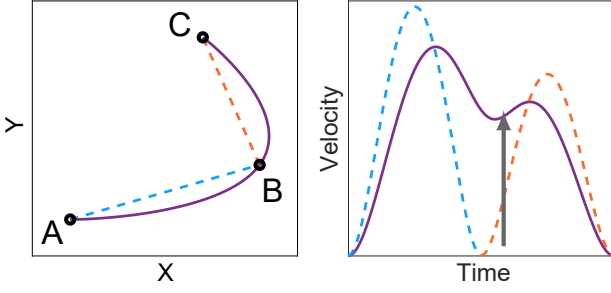
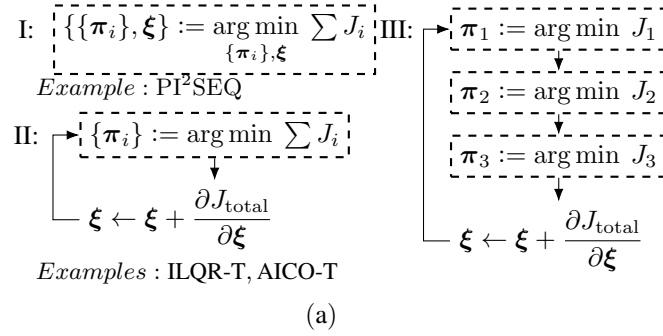


Figure 3. Minimal jerk trajectories AB, BC and a via-point movement AC. AB, BC are both individually minimal jerk trajectories, but simply sequencing them is not optimal for A via B to C. The optimal via-point minimal jerk trajectory is curved around B in the X-Y plane (right).



	I	II	III
Optimize cost function weighting	No	Yes	Yes
Exploit variable impedance	Yes	Yes	Yes
Optimize temporal parameters	Yes	Yes	Yes
Avoid redesign of composite cost function	No	No	Yes

(b)

Figure 4. (a) Three possible types of approaches for sequential movement optimization. Dashed rectangle means a full optimization loop. (b) The table summarizes comparison of type I-III. For simplicity, in Type III only 3 sub-problems are shown to visualize a sequence.

shows an example of exploiting the *redundancy* of velocity profile when concatenating discrete movements.

Based on the above reasoning, it follows that when a sequence is generated by chaining movement primitives, it may be suboptimal without appropriately planning each individual considering the whole trajectory or its subsequent ones. In general, one can structure the problem as a composite optimization or tackle it hierarchically. Depending on whether either way is adopted, or both, there are three possible approaches, as depicted in Figure 4. Throughout this paper, π denotes the control policy, ξ represents vector of policy parameters to be optimized via reinforcement learning, J is used for cost function.

To narrow down our discussion, we mainly consider the applications for (i) optimization of cost function weighting, (ii) exploitation of variable impedance, and (iii) optimising temporal parameters such as the time horizon and relative timing.

To avoid confusion, the sequential movements/tasks considered in this chapter are sequences in a predefined order. The problem of planning the order of executing a set of actions for a given task is not within the scope of

this work. This kind of task planning problem does not predefine an order of executing subtasks. Therefore it needs a higher level planning to figure out the best order to chain the submovements, typically from a discrete set of actions (Manschitz et al. (2015)).

2.2.1 Composite Optimization Composite optimization here means optimizing w.r.t. a composite cost function that consists of the objectives of subtasks. For instance, an optimization-based approach usually consider the via-point problem by defining the cost function as

$$J = (\mathbf{x}(t_v) - \mathbf{x}_v^*)^T \mathbf{H}_v (\mathbf{x} - \mathbf{x}_v^*) + (\mathbf{x}(t_f) - \mathbf{x}_f^*)^T \mathbf{H}_f (\mathbf{x} - \mathbf{x}_f^*) \quad (1)$$

Here \mathbf{x} is the state vector of the problem, $\mathbf{x}_v^*, \mathbf{x}_f^*$ are the via-point and final targets respectively, $\mathbf{H}_v, \mathbf{H}_f$ are diagonal matrices to penalize the deviation, and t_v, t_f represent the fixed via-point time and final time. The optimal control $\mathbf{u}(\mathbf{x}, t) = \pi(\mathbf{x}, t)$ with corresponding policy π is the one that minimizes the cost function. The above minimal jerk via-point problem is one example that has analytical solution (Flash and Hogan (1985)). The shortcoming of this is that if t_v is allowed to be adjusted, the optimization of (1) with a guess about t_v may leads to suboptimal solutions.

Let us first consider the possibility to simultaneously optimize the control and some hyper-parameter like t_v . This is categorized as Type I in Figure 4. For many non-linear real problems arising in robotics, a classical method is to convert the OC problem into a non-linear programming problem. Considering the computational efficiency, a more efficient paradigm for learning control is to transform the representation of the control policies into a lower-dimensional space, and then optimize the policies and their hyper-parameters simultaneously. For example, Stulp et al. (2012) implemented the (model-free) reinforcement learning algorithm PI² for sequential tasks (termed as PI²SEQ), with the help of dynamic motion primitives (DMP) for trajectory encoding using dynamical systems. The shape parameter of trajectories and the attractors of dynamical systems are optimized together, so that the trajectory and its final state is optimized for all subsequent actions. The limitation of composite cost function is that it faces the cost function shaping issue. When competing terms from different subtasks come together, optimality of sub-movements may be no longer achievable. In order to achieve optimality for all subtasks the formulation of the cost functions have to be redesigned.

2.2.2 Hierarchical Optimization The second possible approach is to construct the optimization problem hierarchically. As shown by Type II in Figure 4, it is hierarchical in the sense that an inner loop and an outer loop optimize the control policies and hyper-parameters separately. Various previous studies addressing the multiphase optimal control can be found in this type. To name a few, temporal optimization with Iterative Linear Quadratic Regulator (ILQR-T) and approximate inference (AICO-T) was proposed by Nakanishi et al. (2011) and Rawlik et al. (2010) respectively. Nakanishi et al. (2011) used finite difference to compute the gradient of total cost w.r.t. change of time durations. The evaluation of the gradient is based on running the time-scaled augmented control and hence is very efficient. This

is done by leveraging a technique that maps the real time to a canonical time. It was demonstrated by Rawlik et al. (2010) with similar technique on a via-point task, where the algorithm finds an optimal relative timing. In case J_{total} is non-differentiable w.r.t. ξ , one can utilize derivative-free methods (Conn et al. (2009)) such as trust region technique (Yuan (2015)) and evolutionary strategy (Hansen and Ostermeier (2001)) in the outer loop.

This hierarchical structure coincides with the so-called “bi-level” problem in inverse optimal control (Mombaur et al. (2010)). In inverse optimal control the outer loop optimizes the cost function shaping to match data demonstrated from a human. Of interest here is the fact that the objective J_{total} in the outer loop need not be the same as the composite cost. Suppose that, for the speed and robustness of optimization, the subtasks may be described with simple quadratic terms such as traditional “control effort”, or even have different energetic functions individually, but on the high level, the parameter can be updated according to more realistic cost estimator or physical measurement. This potential can be realized within the bi-level architecture.

Note that, since Type II also employ a composite cost function in the inner loop, it shares the same shortcoming with Type I that composite optimization may fail to achieve optimality for all subtasks and thus need redesign. To overcome the drawback, we propose to optimize the sub-movements according to their own cost function as well as integrate the hierarchical (bi-level) architecture, which leads to Type III (Figure 4). The comparison against previous two types is summarized in the table (Figure 4 (b)).

3 Problem Formulation

In this section we first present a OC model of a single joint driven by a VIA, followed by an investigation of energy efficiency based on the concept of efficient frontiers. The intuition gained thereby helps with justifying the problem formulation. Finally, a reinforcement learning problem is formulated that enables optimizing high-level parameters using policy improvement methods.

3.1 A Simple Reaching Movement Model

Consider a point-to-point fast reaching task using a single-link robot driven by a VIA. The robot used in this paper is MACCEPA Van Ham et al. (2007) with variable damping Radulescu et al. (2012) (VD). As illustrated in Figure 5, the equilibrium position (EP) is controlled with SERVO1 and stiffness is regulated by spring pretension via SERVO2. The mechanism was implemented in our previous work Wu and Howard (2020), where the damping is modulated by controlling a dedicated switching circuit that adjusts back-electromotive force on a DC motor attached to the joint. The system model provided in Appendix A. A fast reaching task

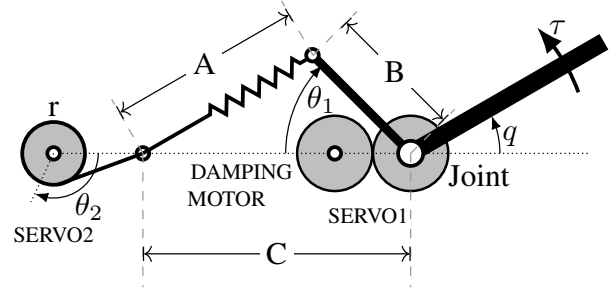


Figure 5. Diagram of MACCEPA-VD (Van Ham et al. (2007); Radulescu et al. (2012)).

is represented by a cost function

$$J(x(\cdot), u(\cdot)) = H(x(t_f)) + \int_0^{t_f} l(x(t), u(t), t) dt \quad (2)$$

$$H(x(t_f)) = 1000(q(t_f) - q^*)^2 \quad (3)$$

$$l(x(t), u(t), t) = 1000(q(t) - q^*)^2 + w_e((u_1(t) - q^*)^2 + u_2^2(t) + 10^{-3}(u_3(t) - 0.5)) \quad (4)$$

An optimal control problem can be formulated as to seek an optimal control $\mathbf{u}(t) \in U \in \mathbb{R}^3$ constrained by its admissible set $U = \{\mathbf{u} \in \mathbb{R}^3 \mid \mathbf{u}_{\min} \preceq \mathbf{u} \preceq \mathbf{u}_{\max}\}$, that minimizes the cost function (2) and subject to the state-space model of the robot dynamics. In the cost function, w_e serves as a weighting parameter to enable adjustment of the performance-cost trade-off.

In addition to trade-off balance via cost function weighting, the stiffness at transition could have a significant influence on the energy efficiency of the subsequent movement. This is explained as follows.

3.2 Efficient Frontiers of Optimal Control

Efficient frontier (EF) is a common tool to examine the trade-off of two competing objectives in an optimization problem. In this work the problem can be interpreted as optimizing the task performance while minimizing the energy cost. The EF is then the set of optimal solutions that achieve the best performance at a defined energy cost. The above OC problem has an efficient frontier by varying the weighting parameter w_e . Then the distribution of optimal solutions can be visualized in performance-cost plane.

In addition, to investigate how pre-stored elastic energy affect the energy efficiency, we generate the optimal solutions by Iterative Linear Quadratic Regulator for different values of w_e , with a certain minimal spring pretension to produce an EF. Multiple EFs are generated by changing the condition of minimal spring pretension. This is done by setting the initial stiffness motor angle $\theta_2(0)$ and the lower bound $u_{\min}^{(2)}$ of u_2 to a preset value p_s , i.e., let $\theta_2(0) = u_2^{\min} = p_s \in P_s := \{p_s \in \mathbb{R} \mid \theta_2^{\min} \leq p_s \leq \theta_2^{\max}\}$.

The results are shown in Figure 6. The vertical axis represents the reaching accuracy performance, which is the terminal cost (3) plus the integral of the first term of running cost (4). The horizontal axis is the energy cost, measured by positive input mechanical work³ E_{in} and electric work E_{elec} , both estimated by simulation.⁴

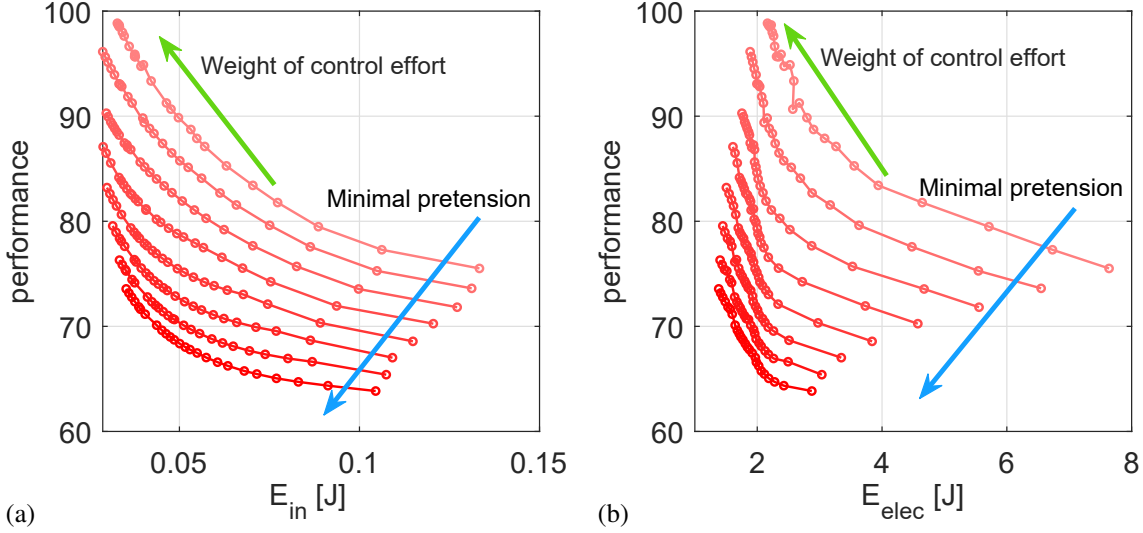


Figure 6. Efficient frontiers : (a) fast reaching performance against input mechanical work, and (b) fast reaching performance against electrical work. Each efficient frontier shows the optimal control solutions by varying the weight w_e of control effort term (shown by the green arrow) in the cost function, with a certain minimal spring pretension. The green arrow indicates the direction of increasing the weight. The spring preset parameter p_s is adjusted by the servo M_2 from 0.1 rad to 1.5 rad with increment of 0.2 rad. Increasing the minimal spring pretension (shown by the blue arrow) moves the efficient frontier downward, which means a increased overall energy efficiency.

$$E_{in} = \int [P_{in1}]^+ + [P_{in2}]^+ dt \quad (5)$$

$$E_{elec} = \int [P_{elec1}]^+ + [P_{elec2}]^+ dt \quad (6)$$

where $[\cdot]^+ = \max(0, \cdot)$. For in-depth analysis of modelling motor energy consumption, we refer the readers to Verstraten et al. (2016). Calculation of the mechanical and electrical power is given in Appendix A.

Looking at Figure 6, when increasing the weight of control effort w_e (as shown by the direction of green arrow), both mechanical and electrical consumption are decreased, with some loss of reaching performance. It demonstrates that even with a simple quadratic control cost, it is still possible to tune the trade-off between performance and realistic energy measures. Moreover, it can be seen in that, by increasing the minimal spring pre-tension p_s , the efficient frontiers move towards the bottom-left, which signals an overall improvement of energy efficiency.

Overall, the above investigation based on the tool of efficient frontier suggests that control cost weight w_e and minimal stiffness p_s can be taken as hyper-parameters that tunes the performance-cost trade-off according to realistic energy measures.

3.3 Reinforcement Learning Formulation

Based on the previous rapid reaching OC model, let us now consider a consecutive reaching task for example, that requires the arm to reach a sequence of targets $\{q_i^*\}_{i=1}^{N_s}$ from initial state \mathbf{x}_0 , where N_s is the number of subtasks. The sequential movement $\mathcal{S} := \{\mathcal{M}_i\}_{i=1}^{N_s}$ consists of N_s sub-movements generated by solving optimal control problem (OCP). The sub-problems is denoted as $\{\text{OCP}_i\}_{i=1}^{N_s}$. We define $\xi \in \{\xi \in \mathbb{R}^{d_p} \mid \xi_{\min} \preceq \xi \preceq \xi_{\max}\}$

to be the stacked vector of weighting parameter $\mathbf{w}_e = \{w_e^{(i)}\}$, stiffness parameter $\mathbf{p}_s = \{p_s^{(i)}\}$, and movement durations $\mathbf{t}_d = \{t_d^{(i)}\}$.⁵ ξ_{\min}, ξ_{\max} are lower and upper bound of ξ . Note that, depending on the type of task at hand, \mathbf{p}_s may have different meaning. For example, as in §3.2 it is used to set the minimal stiffness motor command. By doing so it constrains the minimal elastic energy to be stored and sets a target for the motor.

Our problem is to find an energy optimal trajectory \mathcal{S} and ξ that minimizes energy cost while achieving all sub-goals. Mathematically, it is formulated as to minimize the episodic cost:

$$J(\mathcal{S}) = J_e + \mathcal{C} \cdot \max\{0, J_p - \bar{J}_p\} \quad (7)$$

The cost objective (7) is formulated as an *episodic* cost. J_e is the energy consumption, and J_p is the cost associated with task achievement. The amount of J_p exceeding an upper bound \bar{J}_p is penalized by a large constant \mathcal{C} . The energy consumption can be estimated by a cost function or measured on hardware. \bar{J}_p is evaluated by solving $\{\text{OCP}_i\}$ with initial $\xi^{(0)}$.

4 Method

The policy improvement optimizes J in an iterative process. Figure 7 outlines the paradigm of our proposed policy improvement method which encapsulates OCPs at the low-level. It consists of the main steps of general policy improvement procedures: exploration, evaluation, and policy update. Different from the vanilla reinforcement learning from exploration and evaluation we have an inner loop to solve $\{\text{OCP}_i\}$ sequentially.

The first step is to evaluate the initial trajectory with $\xi^{(0)}$ given by the user. Once $\{\text{OCP}_i\}$ are specified, we run Iterative Linear Quadratic Regulator to generate $\mathcal{S}^{(0)} = \{\mathcal{M}_i\}_{i=1}^{N_s}$ and obtain corresponding costs $J_e^{(0)}, J_p^{(0)}$.⁶ The

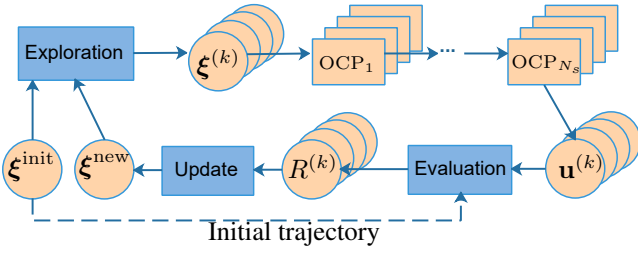


Figure 7. Diagram of proposed policy improvement method.

task performance constraint is set up by multiplying a tolerance factor $\sigma_{tol} \in \{0 \cup \mathbb{R}^+\}$ with $J_p^{(0)}$, i.e., $\bar{J}_p = (1 + \sigma_{tol}) J_p^{(0)}$. The tolerance factor is introduced for user to trade-off the energy efficiency flexibly. A positive value allows the exploration for some samples that have worse performance so that the information may contribute to faster and more robust updating towards the minimal energy cost.

4.1 Exploration and evaluation

The exploration phase generates K unconstrained perturbations in policy parameter space for K roll-outs. The perturbations $\tilde{\epsilon}_k \sim \mathcal{N}(\mathbf{0}, \gamma^{n-1} \Sigma_\epsilon)$, ($k = 1, \dots, K$) is assumed to obey normal distribution, where Σ_ϵ is the covariance matrix and $\gamma \in (0, 1)$ is the decay factor. Then the box constraint $\underline{\mathbf{b}}$ and $\bar{\mathbf{b}}$ is applied to yield

$$\epsilon_k = \min(\max(\tilde{\epsilon}_k + \xi^{(n)}, \xi_{\min}), \xi_{\max}) - \xi^{(n)} \quad (8)$$

$$\xi^{(n)[k]} = \xi^{(n)} + \epsilon_k \quad (9)$$

When running each k -th roll-out, $\xi^{(n)[k]}$ is used to specify sub-problems with \mathbf{w}_e for cost function J_i , \mathbf{p}_s for stiffness motor constraint, and t_d for time horizon. Without loss of generality, we assume the time horizon $[t_0, t_f]$ of i -th sub-problem is from $t_0 = 0$ to $t_f = t_d^{(i)}$.

With these details, $\{\text{OCP}_i\}$ are solved by Iterative Linear Quadratic Regulator sequentially to generate the sub-movements \mathcal{M}_i . The final state of $\mathcal{M}_i = \{\mathbf{x}_i, \mathbf{u}_i\}$ is taken as the initial state of its sequent problem, i.e., $\mathbf{x}_{i+1}(0) = \mathbf{x}_i(t_f^{(0)})$. The energy consumption $J_e^{[k]}$ and task performance $J_p^{[k]}$ along the trajectory is then evaluated by running a forward pass of dynamics and control $\mathbf{u} = \{\mathbf{u}_i\}$. After running K roll-outs and collecting relevant costs, the total costs $J^{[k]}$ are calculated by (7).

4.2 High-level policy update

The policy update step (10)-(12) utilizes the reward-weighted averaging rule as introduced by Stulp and Sigaud (2013).

$$\tilde{J}^{[k]} = \frac{J^{[k]} - \min(\{J^{[k]}\})}{\max(\{J^{[k]}\}) - \min(\{J^{[k]}\})} \quad (10)$$

$$P_k = \frac{\exp(-c\tilde{J}^{[k]})}{\sum_{i=1}^K \exp(-c\tilde{J}^{[i]})} \quad (11)$$

$$\xi \leftarrow \xi + \sum_{k=1}^K P_k \epsilon_k \quad (12)$$

Algorithm 1 Optimization of sequential movements using OC-ES

```

1: Given:  $\{J_i\}, \{\text{OCP}_i\}, \xi_{\min}, \xi_{\max}$ 
2: Initialization:  $\xi^{(0)}, \gamma, \Sigma_\epsilon, \mu, \sigma_{tol}$ 
3: Generate  $\mathcal{S}^{(0)}$  by solving  $\{\text{OCP}_i\}$ , compute  $\bar{J}$ 
4: repeat
5:   for  $k = 1$  to  $K$  do ▷  $k$ -th rollout
6:     Sample  $\tilde{\epsilon}_k \sim \mathcal{N}(\mathbf{0}, \gamma^{n-1} \Sigma_\epsilon)$  ▷ Unconstrained perturbations
7:      $\epsilon_k = \min(\max(\tilde{\epsilon}_k + \xi^{(n)}, \xi_{\min}), \xi_{\max}) - \xi^{(n)}$  ▷ Constrained perturbations
8:      $\xi^{(n)[k]} \leftarrow \xi^{(n)} + \epsilon_k$ 
9:     Specify hyper-parameters and constraints of  $\{\text{OCP}_i\}$  according to  $\xi^{(n)[k]}$ 
10:    for  $i = 1$  to  $N_s$  do
11:       $t_0 = 0, t_f = t_d^{(i)}, \mathbf{x}_i(0) = \mathbf{x}_{i-1}(t_f),$ 
12:      solve  $\{\text{OCP}_i\}, \mathbf{u}_i = \arg \min J_i$ 
13:       $\mathcal{M}_i = \{\mathbf{x}_i, \mathbf{u}_i\}$ 
14:    end for
15:    Estimate  $J_p^{[k]}, J_e^{[k]}$ ,
16:  end for
17:  Retrieve stored samples and append to dataset  $\{J^{[k]}, \epsilon_k\}, K' = K + \mu$ 
18:  Compute and normalize cost  $\{J^{[k]}\}_{k=1}^{K'}$  by (7) (10)
19:  Update  $\xi^{(n+1)}$  using (11) and (12)
20:  Keep  $\mu$  best samples for sample reuse
21: until  $\xi$  converges or maximum number of iterations reached

```

First the cost $J^{[k]}$ is normalized according to their maximum and minimum by (10). The normalized cost $\tilde{J}^{[k]}$ is used to calculate probability P_k for k -th roll-out according to (11), where $c > 0$ is a constant.⁷ Finally, the update is computed by the weighted averaging rule (12).

The above weighted averaging technique is simplified from PI² (Stulp and Sigaud (2013)) and converts the policy improvement method into a black-box optimization (BBO) method that resembles the evolutionary strategy (μ, λ) -ES, which is the basic form of CMA-ES algorithm (Hansen and Ostermeier (2001)). It is appealing because it can solve non-linear non-convex black box optimization problems with reasonable efficiency. Unlike CMA-ES (Hansen and Ostermeier (2001)), it does not have the covariance matrix adaption step. Instead, we manually specify a decay factor γ to gradually decrease the variance of perturbations.

A (μ, λ) -ES method consists of three steps: mutation, selection and recombination. The exploration phase corresponds to the mutation step. Then all samples are selected for policy update (recombination). The policy update step can be viewed as recombination of samples. In contrast to the reinforcement learning algorithm PI² that leverages the problem structure, ES treats the policy improvement as a BBO problem. Since the high-level optimization is solved as a BBO problem in our proposed policy improvement method, we label the high-level part of the whole method as a evolutionary strategy.

For better robustness of convergence, another technique employed is sample reuse. After every update, we keep μ best samples among K roll-outs (at current iteration) for next update. Therefore, after the first iteration, we have

$K + \mu$ samples. The exploration, evaluation and policy update procedures are repeated until ξ converges or reaches maximum steps. The whole algorithm is summarized in Algorithm 1 and termed as OC-ES, which stands for Optimal Control (at low-level) with Evolutionary Strategy (at high-level).

5 Evaluations

Task 1 - consecutive fast reaching To evaluate our proposed method, a consecutive fast reaching task is designed to test on the MACCEPA-VD robot. The task requires the joint actuated by MACCEPA-VD to reach a sequence of three targets $\{q_i^*\}_{i=1}^3 := \{0.7, -0.35, 0.3\}$ (radians) rapidly within a fixed time horizon $T_i = 1$, for $i = 1, 2, 3$, from initial state $\mathbf{x}_0 = (0, 0, 0, \pi/24, 0, 0)^T$. The cost function J_i for each subtask is defined by (2) - (4). A single fast reaching problem was used by Radulescu et al. (2012) to investigate the role of variable damping for VIAs when an appropriate amount of damping is needed to suppress oscillation of movements.

For comparison, a benchmark is generated by using Iterative Linear Quadratic Regulator to solve the sub-problems sequentially. The spring preset $p_s^{(i)} = \pi/24$ rad is the lower bound of stiffness motor position command and weighting parameter $w_e^{(i)} = 1$ for $i = 1, 2, 3$. The resulting (approximately) optimal trajectory \mathcal{S} is denoted by ILQR-0, and used as initial trajectory later for our proposed method.

5.1 Task 1: policy improvement with parametrized trajectory

The competing terms in the composite cost function may hinder the fulfilment of all sub-goals. To investigate this issue we directly optimize the trajectory and stiffness profile simultaneously w.r.t. the composite cost function of **Task 1**

$$J(\mathcal{S}) = \sum_{i=1}^3 J_i(\mathcal{M}_i) \quad (13)$$

$$J_i = 1000 ((q(t_f) - q_i^*)^2 + \dot{q}^2(t_f)) \quad (14)$$

$$+ \int_{t_0}^{t_f} 1000 (q(t) - q_i^*)^2 dt \quad (15)$$

$$+ \int_{t_0}^{t_f} (100 (\theta_1 - q_i^*)^2 + 100 \theta_2^2 + 10^{-3} \theta_3) dt \quad (16)$$

The trajectories are parametrized by DMPs as introduced in Appendix B. Each sub-movement consists of 3 DMPs representing the trajectories of EP motor, stiffness motor and damping command. All DMP are initialized with shaping parameter $\mathbf{w} = \mathbf{0}$, which is a 10 dimensional vector. The goals $\mathbf{g}_1, \mathbf{g}_2, \mathbf{g}_3$, for EP, stiffness motor, and damping respectively, are initialized as $\mathbf{g}_1 = \mathbf{q}^*$, $\mathbf{g}_2 = 24/\pi \mathbf{e}^{(3)}$, $\mathbf{g}_3 = 0.5 \mathbf{e}^{(3)}$,⁸ where $\mathbf{e}^{(d)}$ represents a d -dimensional unit vector. The shaping parameter \mathbf{w} is unconstrained. The box constraints are $[-\pi/3, \pi/3], [\pi/24, \pi/2], [0, 1]$ for elements of $\mathbf{g}_1, \mathbf{g}_2$ and \mathbf{g}_3 respectively. The overall policy parameter ξ is a 99-dimensional stacked vector of \mathbf{g} and \mathbf{w} of all three sub-movements. Relevant meta-parameters of the algorithm are $\gamma = 0.95, \mu = 15, K = 45$ and $\Sigma_e =$

$\text{diag}(10 \mathbf{e}^{(90)}, 0.5 \mathbf{e}^{(9)}) \in \mathbb{R}^{99 \times 99}$. Both goals and shaping parameters \mathbf{w} of DMPs are optimized simultaneously by Algorithm 1 except that it doesn't have an inner loop. The policy update rule used is the same as the weighted averaging method (10)-(12). Different from what suggested by Stulp et al. (2012), where the policy update takes the cost-to-go of sub-movements, we use the episodic cost along whole trajectory for policy update.

The learning results of 10 sessions are illustrated in Figure 8. The policy update gradually converges and final energy cost evaluated by input mechanical work E_{in} is successfully reduced from 0.2674 J of ILQR-0 to 0.1843 ± 0.0204 J. The final trajectory of one learning session shown in Figure 9 demonstrates that an optimized \mathbf{p}_s regulates the pretension at the transition phases. The effectiveness of policy improvement with parametrized trajectories for exploiting variable impedance of VIAs is verified despite some drawbacks. First it can be seen that the learning takes thousands of (trajectory) samples due to high dimensionality of ξ , which makes it less likely to be executed on the physical robot in an online fashion. Secondly, the joint trajectory in Figure 9 slightly but visibly deviated from the first two goals, because the integral term in (15) competes with the terminal cost of its previous movement. To circumvent this issue the composite cost function needs redesign to adjust the cost terms, weights, or impose extra constraints.

5.2 Task 1: sequential reaching with OC-ES

Now we take both weighting and stiffness parameters $\mathbf{w}_e, \mathbf{p}_s$ into account and employ the OC-ES framework. The policy parameter ξ for **Task 1** consists of weights of control effort term and stiffness motor preset of each sub-problem. ξ is initialized as $\{w_e^{(i)} = 1, p_s^{(i)} = \pi/24 \text{ rad}\}_{i=1}^3$. $K = 4$ roll-outs are run for each policy update up to 100 iterations. The exploration noise $\Sigma_e = 0.5 \mathbf{I} \in \mathbb{R}^{6 \times 6}$ and decay factor γ is set to 0.95. The sample reuse parameter is chosen to be $\mu = 3$. The initial trajectory is evaluated to record its energy cost $E_{\text{in}}^{(0)}$ and $J_p^{(0)}$. The latter decides the upper bound constraint of reaching performance \bar{J}_p with tolerance factor $\sigma_{\text{tol}} = 0.1$.

During each roll-out, $w_e^{(i)[k]}$ is used to set the weight of control effort term in (4) for i -th OCP, and $p_s^{(i)[k]}$ specifies the minimal position command u_2^{\min} of the stiffness motor. By doing so, it constrains the minimal pretension upon reaching the target. The sub-problems are solved by Iterative Linear Quadratic Regulator. After each policy update, the movement without perturbation is evaluated to record the learning performance. To verify the improvement of energy saving, both initial and final trajectories are executed on the hardware to record the energy consumption. The results are summarized in Figure 10 where ILQR-ES denotes the final trajectory.

5.2.1 Significant energy reduction The learning curve in Figure 10(a) shows a fast convergence after 50 iterations and very small variations as also shown in Figure 10(b)(c). It demonstrates that the OC-ES method successfully reduced the energy cost of the whole task whilst keeping worst performance cost within tolerance. The mechanical energy cost in simulation is decreased about 44% from that of the initial ILQR-0 trajectory. The electrical consumption

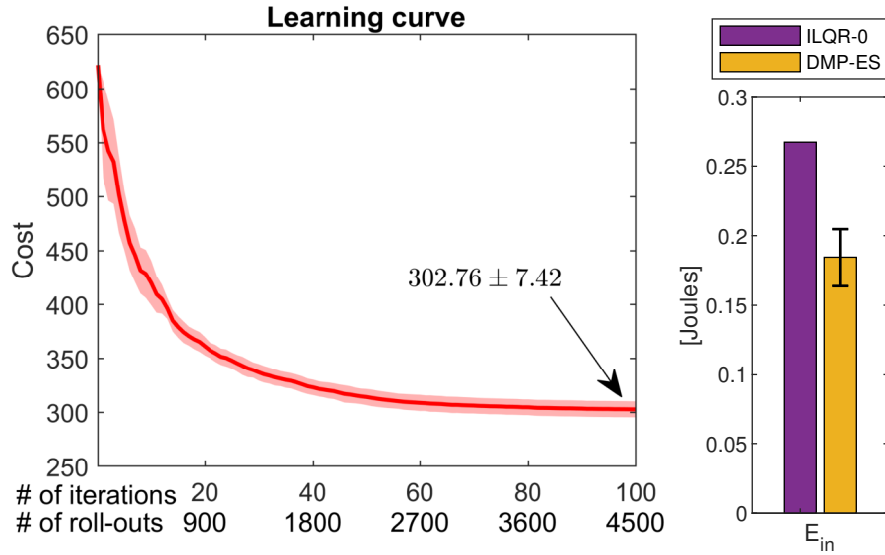


Figure 8. Learning curve (left) of PI^2SEQ for the consecutive fast reaching task. The solid red curve is the mean of 10 runs with shaded area indicating the standard deviation. Comparison of the final energy cost with the ILQR-0 trajectory is plotted in the bar chart (Right). The estimated input energy cost is 0.1843 ± 0.0204 J compared to ILQR-0's 0.2674 J.

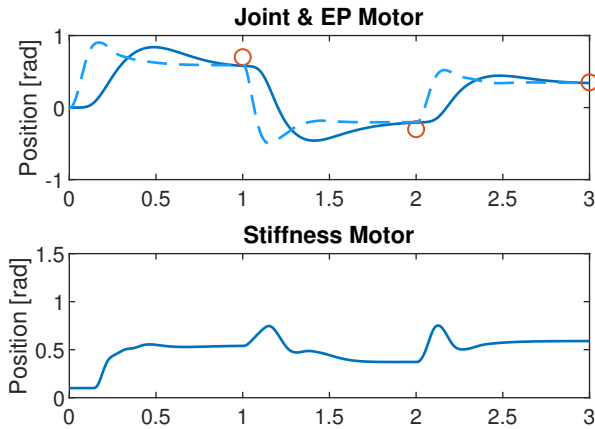


Figure 9. The final trajectory (one of 10 runs) of PI^2SEQ for the consecutive fast reaching task. (Top) Joint (solid) and EP motor (dashed) trajectories, while red dots denote the targets. (Bottom) Stiffness motor trajectory.

recorded on the servomotors verifies the result with a 29.6% reduction.

5.2.2 Optimally tuned cost function weighting Looking at Figure 10(d), all w_e of sub-problems tend to increase from the initial settings. Despite relative large variations of the optimization result, it can be observed that the second sub-movement takes the highest weight for control cost, which indicates the energy efficiency of it is most critical. In Figure 11 we can see that the second sub-movement has the largest travel distance among the three, and consumes the most energy in the initial trajectory (as shown by the accumulated energy cost in the right column in Figure 11). Hence, the result can be explained as the optimization adjusts the weight to balance the performance-cost trade-off more towards reducing energy cost.

5.2.3 Exploiting variable stiffness It can be seen in Figure 11 that energy reduction occurs significantly during the second and third movements, compared with the initial

trajectory. The stiffness motor maintains higher pretension at transition phases (Figure 11(f)) due to the constraint imposed by optimized \mathbf{p}_s , by which the acceleration of the subsequent movement consumes less energy in the EP motor. Also, the adjustment of stiffness motor causes a lot of electrical consumption (Figure 11(h)), suggesting that the control effort may lead to suboptimal solutions regarding real energy consumption. However, this highly depends on the variable stiffness mechanism and hardware design. For example, by implementing the variable stiffness actuators designed for minimizing energy cost for stiffness modulation (Jafari et al. (2015); Chalvet and Braun (2017)), the energy cost of the stiffness motor of initial trajectory can be reduced so that the most saving occurs on the EP motor. However, it would raise another problem that if a variable stiffness actuator does not require energy input to adjust stiffness, then it may not be able to pre-store energy at equilibrium position (EP). As a result there may be no energy buffering effect for some movements starting from a static equilibrium phase.

Overall, the experiment demonstrates the effectiveness of applying OC-ES framework to improve energy efficiency by exploiting variable stiffness and cost function tuning. The learning takes only 4 explorations per iteration by leveraging model-based OC at the low-level, making it more feasible to run on the real robot.

5.3 Temporal and Stiffness Optimization for Tracking Control

The second application is to show that the proposed framework can be applied to temporal optimization and work with a low-level tracking controller.

Task 2 - Consecutive trajectory tracking This task requires the arm to smoothly reach a sequence of targets with minimal-jerk joint trajectory. In addition to exploiting variable stiffness, the relative timing is allowed to be optimized. We set the targets as $\{q_i^*\} = [\pi/5, -0.2, 1, 0.3]$ (rad). The arm starts at $q(0) = 0$ rad. The total time for

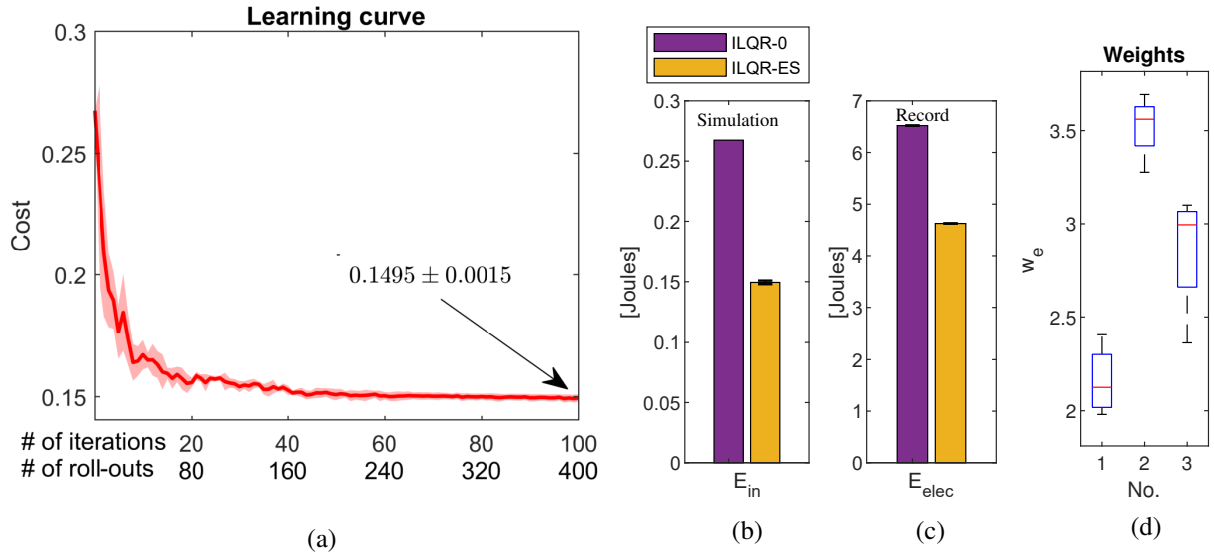


Figure 10. Shown are: (a) Learning curve of ILQR-ES for the consecutive fast reaching task. The solid red curve is the mean of 4 runs with shaded area indicating the standard deviation. (b) Estimated input energy cost of final result is 0.1495 ± 0.0015 J compared to 0.2674 J of ILQR-0. (c) Electrical consumption measured on servomotors is 6.5211 ± 0.2593 J, while the benchmark ILQR-0 consumes 4.6261 ± 0.2812 J, which means a 29.6% reduction. (d) Distribution of optimal w_e for each sub-movement.

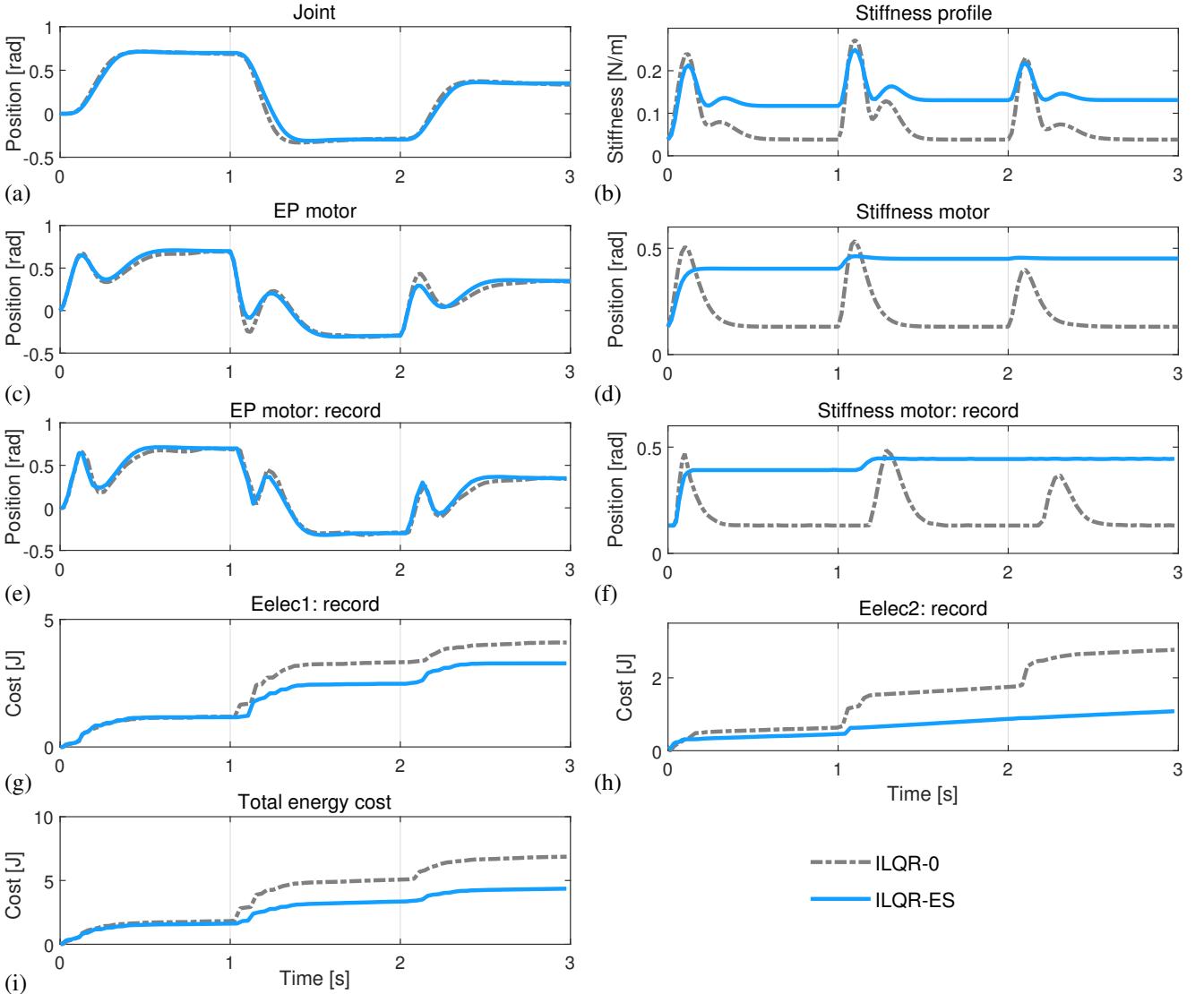


Figure 11. Result of executing the trajectory in simulation and on real hardware of ILQR-ES for consecutive fast reaching, compared with ILQR-0 trajectory as a benchmark. ILQR-0 also serves as the initial trajectory. The last two rows show the measured electrical cost by cumulating the recorded power along the trajectory.

the movement is 2.4 s. ξ is defined as $\xi = (\mathbf{t}_d^\top, \mathbf{p}_s^\top)^\top \in \mathbb{R}^7$, where $\mathbf{t}_d = \{t_d^{(i)}\}_{i=1}^3$, $\mathbf{p}_s = \{p_s^{(i)}\}_{i=1}^4$. Since the total time is kept the same, the last time duration is excluded from the policy parameter. The box constraint on ξ is

$$\begin{aligned}\xi_{\min} &= (0.3, 0.3, 0.3, 0, 0, 0, 0)^\top, \\ \xi_{\max} &= (1.2, 1.2, 1.2, \frac{\pi}{2}, \frac{\pi}{2}, \frac{\pi}{2}, \frac{\pi}{2})^\top\end{aligned}$$

The minimal-jerk joint trajectory can be computed analytically by formula introduced in Flash and Hogan (1985), given the time duration \mathbf{t}_d and where it begins and ends. Then it becomes a joint space tracking problem. The joint tracking with extended inverse dynamics controller (TIDC) derived in Appendix C to track the joint trajectory and resolve the actuation redundancy automatically. The controller serves as a feedback control law and reduces the inner loop OCP to a forward pass of dynamics. The stiffness parameter \mathbf{p}_s is used to impose a constraint on the target position of stiffness motor in each sub-movement, by adding a null-space controller

$$\mathbf{v}_{\text{ns}} = ((q_i^* - \theta_1), p_s^{(i)} - \theta_2, 0)^\top \quad (17)$$

for i -th trajectory tracking. This null-space controller encourages the EP motor to move towards the joint target and the stiffness motor to $p_s^{(i)}$. Other relevant meta-parameters for the policy improvement method are: $K = 10$, $\mu = 3$, $\gamma = 0.97$, $\sigma_{\text{tol}} = 0.01$, $\Sigma_\epsilon = \text{diag}(0.3 \mathbf{e}^{(3)}, 0.5 \mathbf{e}^{(4)})$. The whole method is termed as TIDC-ES.

The initial trajectory is generated with

$$\xi^{(0)} = (0.6, 0.6, 0.6, 0.2, 0.2, 0.2, 0.2)^\top$$

and denoted by TIDC-0. The learning results after 100 iterations are presented in Figure 12. It can be seen that the learning curve initially has a large variation but quickly converges after 40 iterations. Compared to the initial trajectory, by exploiting stiffness and temporal optimization the input mechanical energy E_{in} reduces by about 42%. Looking at the results in Table 1, the optimized stiffness targets range from 1.26 rad for the first sub-movement to nearly 0 rad for the last one. It results in the pretension increasing during the first two sub-movements then decreasing towards the end (as shown in Figure 13). Moreover, the duration of third sub-movement is optimized to 692.6 ms, which is 92.6 ms more than the initial setting. While other three sub-movements have shorter durations. The result is coherent with the order in terms of movement distance.

5.4 Discussion

The experiments presented in this section demonstrated noticeable energy saving realized in consecutive reaching tasks. The task was the same as the one used in Wu and Howard (2020), although there a default spring pretension was chosen manually for all movements.

The proposed method in this paper has been demonstrated to help the robot automatically regulate its stiffness with awareness of subsequent movements. The result of ILQR-ES for Task 1 regulates the stiffness motor to maintain at a small range around 0.5 rad, suggesting that a fixed

value can be tuned for energy efficiency in practice if the movement distances are not distributed diversely. In general, it suggests that for VIAs that rely on spring pretension to modulate stiffness, the more efficient way to use them in consecutive point-to-point reaching is not to reset their stiffness to minimum by default. Hence, using control effort to represent energy cost is questionable as it encourages the stiffness to move towards the minimum at the end of each submovement. However, due to the fact that accurate estimation of $E_{\text{in}}, E_{\text{elec}}$ needs a much smaller time step for discretization of the continuous system dynamics, the quadratic control effort is preferred for less computation cost. It also enhances smoothness of the trajectory, although at a cost to energetic optimality. Nevertheless, this loss is alleviated — by applying the proposed framework — with an upper layer optimizer that adjusts the trade-off balance.

6 Conclusions

This paper proposed a versatile framework that integrates Optimal Control and Evolution Strategy (OC-ES) in a bi-level structure to address the optimization of movement sequence specifically for VIAs. At the low-level OC is leveraged to resolve the actuation redundancy and exploit variable impedance naturally. The high-level optimization in sequential context is formulated as a reinforcement learning problem, in the form of iterative policy improvement, and solved as a black box optimization using method inspired by evolutionary strategy.

The proposed framework was applied for two consecutive reaching tasks on a MACCEPA-VD actuator, one requires reaching as quickly as possible, the other tracks a smooth trajectory in joint space. In both cases natural dynamics is hard to be exploited for energy buffering as in periodic movement. By investigating the performance-cost trade-off via efficient frontiers, it can be seen how cost function weighting and minimal stiffness preset influence the energy efficiency. These two aspects can be addressed in the sequential movement context via the proposed framework, by which variable impedance can be fully exploited and the low-level trade-off is optimally balanced. In addition, a tracking controller that resolves the actuation redundancy was implemented to show the temporal and stiffness optimization at high-level can improve the energy efficiency of low-level sequential tracking control. All the experiments presented in §5 demonstrated significant improvement of energy efficiency in both simulations and on hardware.

However, this work has been limited to reaching movements. More task types need to be considered in the future work to demonstrate more complex behaviours. Furthermore, it would be interesting to extend the application to compliant robots with multiple DOFs and consider problems involving contacts and interactions.

Notes

1. The graphics showing the movements of a human walking and playing basketball are from the book *Classic Human Anatomy in Motion: The Artist's Guide to the Dynamics of Figure Drawing* written by Valerie L. Winslow.
2. When the form of the cost function is determined, the weighting parameter can be adjusted to tune the energy

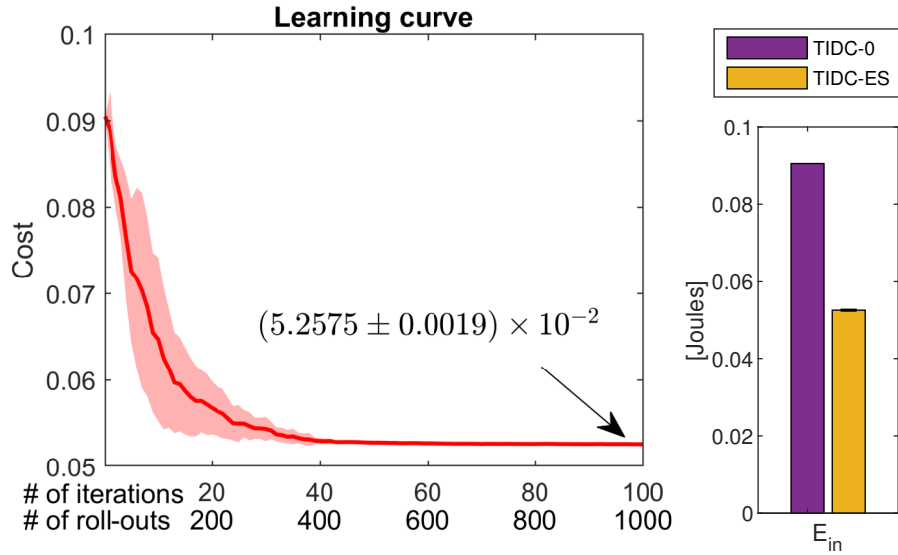


Figure 12. Learning curve (left) of TIDC-ES for the consecutive fast reaching task. The solid red curve is the mean of 10 runs with shaded area indicating the standard deviation. Comparison of the final energy cost with the TIDC-0 trajectory is plotted in the bar chart (right). The estimated input energy cost is $(5.2575 \pm 0.0019) \times 10^{-2}$ J compared to TIDC-0's 9.054×10^{-2} J.

Optimized parameters				
No.	1	2	3	4
$t_d^{(i)}$ [ms]	555.8 ± 5.1	593.1 ± 2.5	692.6 ± 3.4	558.5 ± 1.6
$p_s^{(i)}$ [rad]	1.259 ± 0.013	0.782 ± 0.007	0.412 ± 0.008	0.002 ± 0.002

Table 1. Optimized parameters of temporal and stiffness optimization with TIDC-ES.

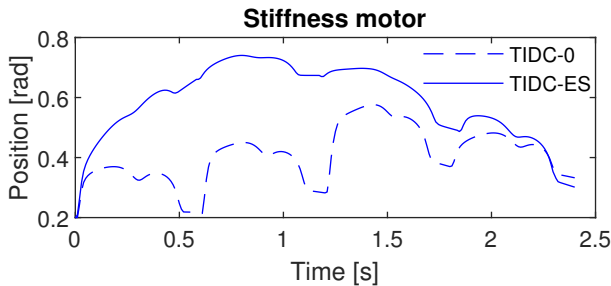


Figure 13. Stiffness motor profile of TIDC-ES final trajectory (blue solid) compared to initial trajectory (dashed blue).

efficiency. For simple quadratic control effort, the weight for each sub-movement need not be the same and can be optimized according to realistic energetics (by estimation or measurement).

3. We assume that the motors are not back-drivable, thus no negative mechanical work to the motors can be regenerated. Similarly, the electrical energy is defined as the integral of the positive part.
4. Note that, the accuracy of estimating E_{in} , E_{elec} is very sensitive to simulation step size. For Iterative Linear Quadratic Regulator we typically use time step $\Delta t = 0.02$. While computing E_{in} , E_{elec} is based on simulation (of forward dynamics) with $\Delta t = 0.001$.
5. By convention, all vector quantities are assumed to be column vectors.
6. For the initial trajectory, it is obvious that $J^{(0)} = J_e^{(0)}$
7. In our implementation we choose $c = 10$.
8. \mathbf{g}_2 here is actually \mathbf{p}_s .

References

- Ariani G and Diedrichsen J (2019) Sequence learning is driven by improvements in motor planning. *Journal of Neurophysiology* 121(6): 2088–2100. DOI:10.1152/jn.00041.2019.
- Berret B, Ivaldi S, Nori F and Sandini G (2011) Stochastic optimal control with variable impedance manipulators in presence of uncertainties and delayed feedback. *IEEE International Conference on Intelligent Robots and Systems* : 4354–4359 DOI:10.1109/IROS.2011.6048586.
- Bobbett MF (2001) Dependence of human squat jump performance on the series elastic compliance of the triceps surae: A simulation study. *Journal of Experimental Biology* 204(3): 533–542.
- Braun D, Howard M and Vijayakumar S (2012) Optimal variable stiffness control: formulation and application to explosive movement tasks. *Autonomous Robots* 33(3): 237–253.
- Braun D, Petit F, Huber F, Haddadin S, Van Der Smagt P, Albu-Schaffer A and Vijayakumar S (2013) Robots driven by compliant actuators: Optimal control under actuation constraints. *IEEE Transactions on Robotics* 29(5): 1085–1101.
- Burridge RR, Rizzi AA and Koditschek DE (1999) Sequential composition of dynamically dexterous robot behaviors. *International Journal of Robotics Research* 18(6): 534–555. DOI:10.1177/02783649922066385.
- Chalvet V and Braun DJ (2017) Criterion for the Design of Low-Power Variable Stiffness Mechanisms. *IEEE Transactions on Robotics* 33(4): 1002–1010. DOI:10.1109/TRO.2017.2689068.
- Conn AR, Scheinberg K and Vicente LN (2009) *Introduction to Derivative-Free Optimization*. SIAM.

- Flash T and Hogan N (1985) The coordination of arm movements: an experimentally confirmed mathematical model. *The Journal of neuroscience* 5(7): 1688–703. DOI:4020415.
- Haddadin S, Krieger K, Albu-Schaffer A and Lilge T (2018) Exploiting elastic energy storage for blind cyclic manipulation: Modeling, stability analysis, control, and experiments for dribbling. *IEEE Transactions on Robotics* 34(1): 91–112.
- Hansen N and Ostermeier A (2001) Completely Derandomized Self-Adaptation in Evolution Strategies. *Evolutionary Computation* 9(2): 159–195. DOI:10.1162/106365601750190398.
- Hogan N and Sternad D (2012) Dynamic primitives of motor behavior. *Biological Cybernetics* 106(11-12): 727–739. DOI: 10.1007/s00422-012-0527-1.
- Huang HJ, Kram R and Ahmed AA (2012) Reduction of Metabolic Cost during Motor Learning of Arm Reaching Dynamics. *The Journal of Neuroscience* 32(6): 2182–2190. DOI:10.1523/JNEUROSCI.4003-11.2012.
- Ijspeert A, Nakanishi J and Schaal S (2002) Movement imitation with nonlinear dynamical systems in humanoid robots. *IEEE International Conference on Robotics and Automation* (May): 1398–1403.
- Ijspeert AJ, Nakanishi J, Hoffmann H, Pastor P and Schaal S (2013) Dynamical movement primitives: learning attractor models for motor behaviors. *Neural computation* 25(2): 328–73.
- Jafari A, Tsagarakis N and Caldwell D (2015) Energy efficient actuators with adjustable stiffness: a review on awas, awas-ii and compact vsa changing stiffness based on lever mechanism. *Industrial Robot: An International Journal* 42(3): 242–251. DOI:10.1108/IR-12-2014-0433.
- Lashley KS (1951) The problem of serial order in behavior. In: *Cerebral mechanisms in behavior; the Hixon Symposium*. Oxford, England: Wiley, pp. 112–146.
- Lay B, Sparrow W, Hughes K and O'Dwyer N (2002) Practice effects on coordination and control, metabolic energy expenditure, and muscle activation. *Human Movement Science* 21: 807–830. DOI:10.1016/S0167-9457(02)00166-5.
- Levine S and Koltun V (2012) Continuous inverse optimal control with locally optimal examples. *Proceedings of the 29th International Conference on Machine Learning, ICML 2012* 1: 41–48.
- Li W and Todorov E (2004) Iterative Linear Quadratic Regulator Design for Nonlinear Biological Movement Systems. In: *IEEE Int. Conf. Robotics & Automation*.
- Lucia P, Umezawa K, Nakamura Y and Billard A (2013) Learning Robot Skills Through Motion Segmentation and Constraints Extraction. In: *HRI Workshop on Collaborative Manipulation*.
- Manschitz S, Kober J, Gienger M and Peters J (2015) Learning movement primitive attractor goals and sequential skills from kinesthetic demonstrations. *Robotics and Autonomous Systems* 74: 97–107. DOI:10.1016/j.robot.2015.07.005.
- Matsusaka K, Uemura M and Kawamura S (2016) Realization of highly energy efficient pick-and-place tasks using resonance-based robot motion control. *Advanced Robotics* 30(9): 608–620.
- Mombaur K, Truong A and Laumond JP (2010) From human to humanoid locomotion—an inverse optimal control approach. *Autonomous Robots* 28(3): 369–383. DOI:10.1007/s10514-009-9170-7.
- Motegi M and Matsui T (2011) Optimal Control Model for Reproducing Squat Movements Based on Successive-Movement Combination. *The Proceedings of the Symposium on sports and human dynamics* 2011: 558–563. DOI:10.1299/jsmeshd.2011.558.
- Nakanishi J, Radulescu A, Braun DJ and Vijayakumar S (2016) Spatio-temporal stiffness optimization with switching dynamics. *Autonomous Robots* : 1–19.
- Nakanishi J, Rawlik K and Vijayakumar S (2011) Stiffness and temporal optimization in periodic movements: An optimal control approach. In: *IEEE/RSJ International Conference on Intelligent Robots and Systems*, 1. pp. 718–724.
- Nelson WL (1983) Physical principles for economies of skilled movements. *Biological cybernetics* 46: 135–147. DOI:10.1007/BF00339982.
- Okada M, Ban S and Nakamura Y (2002) Skill of compliance with controlled charging/discharging of kinetic energy. In: *Proceedings 2002 IEEE International Conference on Robotics and Automation (Cat. No.02CH37292)*, volume 3. IEEE. ISBN 0-7803-7272-7, pp. 2455–2460. DOI:10.1109/ROBOT.2002.1013600.
- Radulescu A, Howard M, Braun DJ and Vijayakumar S (2012) Exploiting variable physical damping in rapid movement tasks. In: *IEEE/ASME Int. Conf. Advanced Intelligent Mechatronics*.
- Rawlik K, Toussaint M and Vijayakumar S (2010) An Approximate Inference Approach to Temporal Optimization in Optimal Control. *Neural Information Processing Systems* : 1–9.
- Reher J, Cousineau EA, Hereid A, Hubicki CM and Ames AD (2016) Realizing dynamic and efficient bipedal locomotion on the humanoid robot durus. In: *2016 IEEE International Conference on Robotics and Automation (ICRA)*. pp. 1794–1801. DOI:10.1109/ICRA.2016.7487325.
- Roberts TJ (2016) Contribution of elastic tissues to the mechanics and energetics of muscle function during movement. *The Journal of Experimental Biology* 219(2): 266–275. DOI:10.1242/jeb.124446.
- Roozing W, Li Z, Caldwell DG and Tsagarakis NG (2016) Design Optimisation and Control of Compliant Actuation Arrangements in Articulated Robots for Improved Energy Efficiency. *IEEE Robotics and Automation Letters* 1(2). DOI: 10.1109/LRA.2016.2521926.
- Roozing W, Ren Z and Tsagarakis NG (2019) An efficient leg with series-parallel and biarticular compliant actuation: design optimization, modeling, and control of the eLeg. *International Journal of Robotics Research* DOI:10.1177/0278364919893762.
- Schaal S (2006) Dynamic Movement Primitives – A Framework for Motor Control in Humans and Humanoid Robotics. *Adaptive Motion of Animals and Machines* (1): 261–280. DOI:10.1007/4-431-31381-8_23.
- Schaal S and Atkeson CG (2010) Learning control in robotics. *IEEE Robotics and Automation Magazine* 17(2): 20–29. DOI: 10.1109/MRA.2010.936957.
- Sparrow W and Newell KM (1998) Metabolic energy expenditure and the regulation of movement economy. *Psychonomic Bulletin & Review* 5(2): 173–196.
- Stulp F and Sigaud O (2013) Robot Skill Learning: From Reinforcement Learning to Evolution Strategies. *Paladyn, Journal of Behavioral Robotics* 4(1). DOI:10.2478/pjbr-2013-0003.

- Stulp F, Theodorou EA and Schaal S (2012) Reinforcement Learning With Sequences of Motion Primitives for Robust Manipulation. *IEEE Transactions on Robotics* 28(6): 1360–1370.
- Tassa Y, Mansard N and Todorov E (2014) Control-limited differential dynamic programming. In: *ICRA*. pp. 1168–1175.
- Theodorou E, Buchli J and Schaal S (2010) A generalized path integral control approach to reinforcement learning. *J. Mach. Learn. Res.* 11: 3137–3181.
- Todorov E and Jordan M (2002) Optimal feedback control as a theory of motor coordination. *Nature Neuroscience* (5): 1226–1235. DOI:https://doi.org/10.1038/nn963.
- Toussaint M, Gienger M and Goerick C (2007) Optimization of sequential attractor-based movement for compact behaviour generation. In: *2007 7th IEEE-RAS International Conference on Humanoid Robots*, 2. IEEE. ISBN 978-1-4244-1861-9, pp. 122–129. DOI:10.1109/ICHR.2007.4813858.
- Tsagarakis NG, Morfeý S, Medrano Cerda G, Zhibin L and Caldwell DG (2013) Compliant humanoid coman: Optimal joint stiffness tuning for modal frequency control. In: *2013 IEEE International Conference on Robotics and Automation*. pp. 673–678.
- Van Ham R, Vanderborght B, Van Damme M, Verrelst B and Lefeber D (2007) MACCEPA, the mechanically adjustable compliance and controllable equilibrium position actuator: Design and implementation in a biped robot. *Rob. Auton. Syst.* 55(10): 761–768. DOI:10.1016/j.robot.2007.03.001.
- Verstraten T, Furnemont R, Mathijssen G, Vanderborght B and Lefeber D (2016) Energy Consumption of Geared DC Motors in Dynamic Applications: Comparing Modeling Approaches. *IEEE Robotics and Automation Letters* 1(1): 524–530. DOI: 10.1109/LRA.2016.2517820.
- Wilson JM and Flanagan EP (2008) The Role of Elastic Energy in Activities with High Force and Power Requirements: A Brief Review. *Journal of Strength and Conditioning Research* 22(5): 1705–1715. DOI:10.1519/JSC.0b013e31817ae4a7.
- Wolf S and Hirzinger G (2008) A new variable stiffness design: Matching requirements of the next robot generation. In: *2008 IEEE International Conference on Robotics and Automation*. IEEE, pp. 1741–1746.
- Wu F and Howard M (2020) Energy regenerative damping in variable impedance actuators for long-term robotic deployment. *IEEE Transactions on Robotics* : 1–13.
- Yokoi A and Diedrichsen J (2019) Neural Organization of Hierarchical Motor Sequence Representations in the Human Neocortex. *Neuron* 103(6): 1178 – 1190.e7. DOI:https://doi.org/10.1016/j.neuron.2019.06.017.
- Yuan Yx (2015) Recent advances in trust region algorithms. *Mathematical Programming* 151(1): 249–281. DOI:10.1007/s10107-015-0893-2.

Appendix A: The robot model

The forward dynamics of MACCEPAVD can be written as:

$$\ddot{q} = (\tau_s - d(u_3)\dot{q} - b\dot{q} - \tau_{\text{ext}})m^{-1} \quad (18)$$

$$\ddot{\theta}_1 = \beta^2(u_1 - \theta_1) - 2\beta\dot{\theta}_1 \quad (19)$$

$$\ddot{\theta}_2 = \beta^2(u_2 - \theta_2) - 2\beta\dot{\theta}_2 \quad (20)$$

where q, \dot{q}, \ddot{q} are the joint angle, velocity and acceleration, respectively, b is the viscous friction coefficient for the joint, m is the link inertia, τ_s is the torque generated by the spring force, and τ_{ext} is the joint torque due to external loading (the following reports results for the case of no external loading, i.e., $\tau_{\text{ext}} = 0$). $\theta_1, \theta_2, \dot{\theta}_1, \dot{\theta}_2, \ddot{\theta}_1, \ddot{\theta}_2$ are the motor angles, velocities and accelerations.

The motor angles θ_1, θ_2 and damping d are controlled by control input $\mathbf{u} = (u_1, u_2, u_3)^\top$. The servomotor dynamics (19), (20) are assumed to behave as a critically damped system, with β constraining the maximum acceleration of the 2nd order dynamical system.

The torque τ_s can be calculated as follows:

$$\tau_s = \kappa BC \sin(\theta_1 - q) \left(1 + \frac{r\theta_2 - |C - B|}{A(q, \theta_1)}\right) \quad (21)$$

$$\tau_{l1} = \tau_s \quad (22)$$

$$\tau_{l2} = \kappa(r\theta_2 - |C - B| + A(q, \theta_1)) \quad (23)$$

where $A(q, \theta_1) = \sqrt{B^2 + C^2 - 2BC \cos(\theta_1 - q)}$, B and C are the lengths shown in Figure 5, r is the radius of the winding drum used to adjust the spring pre-tension, and κ is the linear spring constant.

The damping coefficient $d(u_3)$ linearly depends on control input u_3 and

$$d(u_3) = \bar{d}u_3, \quad (24)$$

where \bar{d} is maximum damping coefficient and the control input varies from 0 to 1 ($u_3 \in [0, 1]$).

The mechanical and electrical power of motor i are estimated by

$$P_{\text{in},i} = \tau_{l,i}\dot{\theta}_i \quad (25)$$

$$P_{\text{elec},i} = \left(\frac{\tau_{m,i}}{n_g k}\right)^2 R_m + [J_m \ddot{\theta}_i \dot{\theta}_i]^+ + b_f \dot{\theta}_i^2 + [\tau_{l,i} \dot{\theta}_i]^+ \quad (26)$$

$$\tau_{m,i} = \tau_{l,i} + J_m \ddot{\theta}_i + b_f \dot{\theta}_i \quad (27)$$

On the hardware, SERVO1 and SERVO2 are two Robotis Dynamixel XM430-210-R servomotors with internal position and current sensors. The sensing data is transmitted from servos to a PC hosting connected with a dedicated U2D2 USB converter. The communication between servos and PC is based on ROS messages.

The corresponding state-space model for optimal control can be written as

$$\mathbf{f} = \begin{cases} x_2 \\ (\tau_s(x_1, x_2, x_3) - (d(u_3) + b)x_2)m^{-1} \\ x_5 \\ x_6 \\ \beta^2(u_1 - x_3) - 2\beta x_5 \\ \beta^2(u_2 - x_4) - 2\beta x_6 \end{cases} \quad (28)$$

where $\mathbf{x} = (x_1, x_2, x_3, x_4, x_5, x_6)^\top = (q, \dot{q}, \theta_1, \theta_2, \dot{\theta}_1, \dot{\theta}_2)^\top \in \mathbb{R}^6$ is the state vector, $\mathbf{u} = (u_1, u_2, u_3)^\top \in \mathbb{R}^3$ is the control input.

Appendix B: Dynamic Movement Primitives

A widely-used formalization is Dynamic Movement Primitive (DMP) proposed by Schaal (2006) and Ijspeert et al.

(2002, 2013), based on the idea of modelling movements using dynamical systems. Below is a formalization of DMPs for representing actuator variables $\theta = (\theta_1, \theta_2, \theta_3)^T$ represents the EP, stiffness motor and damping profile.

$$\tau \dot{\theta} = \mathbf{z} \quad (29)$$

$$\tau \dot{\mathbf{z}} = \alpha_z (\beta_z (\mathbf{g} - \theta) - \mathbf{z}) + s \mathbf{A}^T \mathbf{f}^\theta(s) \quad (30)$$

$$\tau \dot{s} = -\alpha_s s \quad (31)$$

$$f_m^\theta(s) = \frac{\sum_{i=1}^N \psi_i(s)}{\sum_{i=1}^N \psi_i(s)} w_{m,i} \quad (32)$$

$$\psi_i(s) = \exp\left(-\frac{(s - c_i)^2}{2\sigma_i^2}\right) \quad (33)$$

where $\tau > 0$ represents the duration and \mathbf{g} is the goal position of θ , the dynamics of θ is regulated by a dynamical system which behaves like a mass-spring-damper model, with gains determined by α_z, β_z . $\mathbf{f}^\theta(s)$ is a forcing term manipulating the shape of the trajectory. It is a function in phase variable s , whose dynamics makes it asymptotically converge to 0, in a rate controlled by α_s . As a result, The efficacy of forcing term gradually decays to zero. This behaviour is purposely designed in Ijspeert et al. (2002, 2013) to enhance convergence of θ to the goal \mathbf{g} . In addition to s , \mathbf{A} is added to the forcing term to scale it according to the movement distance, where the m -th element $a_m = g_m - \theta_m$ corresponds to m -th forcing element f_m^θ . From (32) and (33) we can see that the forcing term is defined as the weighted sum of a set of N basis functions, of which each is an exponential function defined by centre point c_i and width factor σ_i .

Appendix C: Tracking joint trajectory with inverse dynamics controller

The controller here is general for multiple DOFs. \mathbf{q} is the joint configuration vector. Suppose that the robot is asked to track a desired trajectory $\{\mathbf{q}_{\text{des}}, \dot{\mathbf{q}}_{\text{des}}, \ddot{\mathbf{q}}_{\text{des}}\}$ and satisfies

$$(\ddot{\mathbf{q}} - \ddot{\mathbf{q}}_{\text{des}}) + \mathbf{K}_3(\dot{\mathbf{q}} - \dot{\mathbf{q}}_{\text{des}}) + \mathbf{K}_2(\mathbf{q} - \mathbf{q}_{\text{des}}) = \mathbf{0} \quad (34)$$

Then taking derivatives of

$$\mathbf{M}(\mathbf{q})\ddot{\mathbf{q}} + \mathbf{C}(\mathbf{q}, \dot{\mathbf{q}})\dot{\mathbf{q}} + \mathbf{G}(\mathbf{q}) = \tau_a(\mathbf{q}, \theta) \quad (35)$$

yields

$$\mathbf{M}\ddot{\mathbf{q}} + \frac{\partial \mathbf{M}}{\partial t}\dot{\mathbf{q}} + \mathbf{C}\ddot{\mathbf{q}} + \frac{\partial \mathbf{C}}{\partial t}\dot{\mathbf{q}} + \frac{\partial \mathbf{G}}{\partial t} = \mathbf{J}_\theta \dot{\theta} + \mathbf{J}_q \dot{\mathbf{q}} + \mathbf{J}_{\dot{\mathbf{q}}} \ddot{\mathbf{q}}. \quad (36)$$

where $\mathbf{J}_\theta, \mathbf{J}_q, \mathbf{J}_{\dot{\mathbf{q}}}$ are used to represent the Jacobians of τ_a w.r.t. $\theta, \mathbf{q}, \dot{\mathbf{q}}$. For the following derivation we assume that θ is controlled in velocity domain by \mathbf{v} .

Combining (34) and (36), after rearranging them, we get

$$\begin{aligned} \mathbf{J}_\theta \mathbf{v} = & \mathbf{M}\ddot{\mathbf{q}}_{\text{des}} - \mathbf{J}_q \dot{\mathbf{q}} - \mathbf{J}_{\dot{\mathbf{q}}} \ddot{\mathbf{q}} + \mathbf{C}\ddot{\mathbf{q}} \\ & + \frac{\partial \mathbf{M}}{\partial t}\dot{\mathbf{q}} + \frac{\partial \mathbf{C}}{\partial t}\dot{\mathbf{q}} + \frac{\partial \mathbf{G}}{\partial t} \\ & + \mathbf{M}(\mathbf{K}_3(\ddot{\mathbf{q}} - \ddot{\mathbf{q}}_{\text{des}}) + \mathbf{K}_2(\dot{\mathbf{q}} - \dot{\mathbf{q}}_{\text{des}}) + \mathbf{K}_1(\mathbf{q} - \mathbf{q}_{\text{des}})) \end{aligned} \quad (37)$$

Denote the right-hand side as \mathbf{b} , given a cost metric matrix \mathbf{N} , the control law can be given as

$$\begin{aligned} \mathbf{u} = & \mathbf{N}^{-\frac{1}{2}} (\mathbf{J}_\theta \mathbf{N}^{-\frac{1}{2}})^\dagger \mathbf{b} \\ & + \mathbf{N}^{-\frac{1}{2}} (\mathbf{I} - (\mathbf{J}_\theta \mathbf{N}^{-\frac{1}{2}})^\dagger \mathbf{J}_\theta \mathbf{N}^{-\frac{1}{2}}) \mathbf{N}^{\frac{1}{2}} \mathbf{u}_1 \end{aligned} \quad (38)$$

which is a closed form controller with joint feedback.